Title
NEW TEST OF TIME REVERSAL INVARIANCE IN 19Ne BETA DECAY

Authors
Calaprice, F.P.
Commins, E.D.
Girvin, D.C.

Publication Date
1973-06-01

Submitted to Physical Review

LBL-2030
Preprint c.1

NEW TEST OF TIME REVERSAL INVARIANCE IN ^{19}Ne BETA DECAY

F. P. Calaprice, E. D. Commins, and D. C. Girvin

June 1973

Prepared for the U. S. Atomic Energy Commission
under Contract W-7405-ENG-48

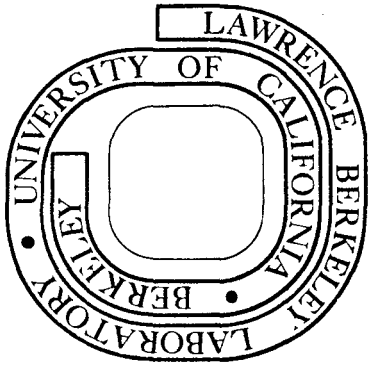

LBL-2030
c.1

DISCLAIMER

New Test of Time Reversal Invariance in ^{19}Ne Beta Decay*

F. P. Calaprice†, E. D. Commins, and D. C. Girvin
Physics Department and Lawrence Berkeley Laboratory
University of California, Berkeley, California

ABSTRACT

A new experimental upper limit on the "time reversal" coefficient D is reported for the allowed beta decay $^{19}Ne \rightarrow {}^{19}Fe^{+}\nu_e$. The result, expressed in terms of the relative phase angle between axial-vector (A) and vector (V) couplings, is $\phi_{A,V}(^{19}Ne) = 180.1 \pm 0.3°$, consistent with T-invariance.

A nuclear-spin-polarized atomic beam of ^{19}Ne in which either of the magnetic substates $m_I = \pm 1/2$ can be selected, is allowed to terminate its flight in a cell, where the ^{19}Ne atoms remain for approximately 4 seconds without substantial spin depolarization. Delayed coincidences between positrons and ^{19}F-recoil ions from decays in the cell are observed and correlated with nuclear spin to determine D. The ^{19}Ne nuclear polarization is monitored continuously by observation of the beta decay asymmetry.

* Work supported by USAEC

† Present address: Physics Dept., Princeton University, Princeton, New Jersey

I. Introduction

We report here an improved experimental test of time reversal (T) invariance in the allowed beta decay:

$$^{19}Ne \rightarrow {}^{19}F^{-} + e^{+} + \nu_e \qquad (t_{\frac{1}{2}} = 17.36 \text{ sec})$$

in which a search is made for a "triple" correlation of the form $\underset{\sim}{J} \cdot \underset{\sim}{p}_e \times \underset{\sim}{p}_\nu$ between the initial nuclear spin and the momenta of the final leptons.[1] In an earlier experiment [2,3] the search was carried out by observations of delayed coincidences between $^{19}F^{-}$ recoil ions and positrons, from the decay-in-flight of a polarized atomic beam of ^{19}Ne. Similar experiments have also been performed with polarized beams of neutrons.[4]

In the present work, the polarized ^{19}Ne beam is allowed to terminate its flight in a cell, where the atoms remain for approximately 4 seconds without suffering appreciable nuclear-spin-depolarization. Observations of decays in the cell yield determinations of the positron asymmetry and neutrino asymmetry as well as the triple correlation. In the latter 2 cases the long cell sitting-time allows greatly enhanced counting rates as compared to those obtained with decays in flight. Thus we have been able to achieve a 5-fold improvement in the precision of the triple correlation measurement.

The experiment may be understood from consideration of the differential transition probability $d\lambda$ for decay of polarized ^{19}Ne, (nuclear spin $J = 1/2$). Using the approximation where all final-state-electromagnetic corrections and momentum-transfer-dependent terms in the beta decay matrix element are neglected, and summing over final lepton spins, we have:

$$d\lambda = \frac{G^2\cos^2\theta}{(2\pi)^5} F(Z,E) \quad (E_0-E)^2 pE dE d\Omega_e d\Omega_\nu$$

$$\{ 1 + a_0 \underset{\sim}{v} \cdot \underset{\sim}{\hat{q}} + \frac{\langle \underset{\sim}{J} \rangle}{J} \cdot [A \underset{\sim}{\chi} + B\underset{\sim}{\hat{q}} + D \underset{\sim}{\chi}\times\underset{\sim}{\hat{q}}] \} \qquad (1)$$

Here we employ units where $\hbar = c = 1$. Also, G is the Fermi coupling constant, θ is Cabibbo's angle, F(Z,E) is the positron spectrum Coulomb correction, and E_0 is the maximum e^+ energy, while p, v, and E are the positron momentum, velocity and energy, respectively. Also, $\hat{q}$ is a unit vector in the direction of neutrino momentum, $d\Omega_e$ and $d\Omega_\nu$ are differential solid angles for positron and neutrino, respectively, and $\langle J\rangle/J$ defines the initial nuclear polarization. Quantities ξ, A, B, and D are given by the formulae:

$$\xi = |a|^2 + |c|^2 \tag{2}$$

$$A = \frac{+\frac{2}{3}|\rho|^2 + \frac{2}{\sqrt{3}}\rho\cos\phi}{1 + |\rho|^2}, \tag{3}$$

$$B = \frac{-\frac{2}{3}|\rho|^2 + \frac{2}{\sqrt{3}}\rho\cos\phi}{1 + |\rho|^2}, \tag{4}$$

$$D = \frac{-\frac{2}{\sqrt{3}}|\rho|\sin\phi}{1 + |\rho|^2}, \tag{5}$$

where $a = C_V M_F$, $c = C_A M_{GT}$, and $\rho \equiv |\rho|e^{i\phi} = a/c$. For $|\rho| = 1.60 \pm 0.01$ as determined from ft (^{19}Ne) we find $D = (.519 \pm .001)\sin\phi$.

From previous measurements it is already known that $\phi \simeq \pi$. Time reversal invariance requires ρ to be real, hence $D = 0$, when final state corrections are neglected. Equations 1-5 have been generalized by Holstein[6], who has considered corrections due to momentum-dependent terms and final state electromagnetic effects. The corrections to ξ, A, and B are negligible for our purposes. In the case of D, our experimental result is

$$D_{expt}\ (^{19}\text{Ne}) = .001 \pm .003 \tag{6}$$

so that the corrections are not negligible a priori. In fact, Holstein finds a contribution of about 2×10^{-4} to D arising from final state effects, in agreement with earlier estimates.[3] As for momentum dependent terms, Holstein has shown that

$$\bar{D}(^{19}\mathrm{Ne}) \simeq \left(\frac{1}{3}\right)^{\frac{1}{2}} \frac{1}{|a|^2+|c|^2} \operatorname{Im} a^*\left(2c + \frac{E_0}{M} d\right) \qquad (7)$$

where $M = 1/2(M(^{19}\mathrm{Ne}) + M(^{19}\mathrm{F}))$, d is the so-called induced tensor contribution to the hadronic weak current matrix element, the validity of the CVC hypothesis is assumed, and the bar over D indicates an average over the e^+ energy spectrum. (See Fig. 11). Equation (7) is identical to equation (5) except for the additional term in d.

Note that for a mirror transition such as $^{19}\mathrm{Ne} \to {}^{19}\mathrm{F}$, the terms a and c are first-class, while d is second-class - with respect to G-parity transformations.[7] As pointed out by Kim and Primakoff and others,[8] the charge-symmetry condition then implies that $\operatorname{Im} a^* c = 0$ even if T-invariance is violated. If this is the case, then a non-zero D could only arise from a non-zero value of $\operatorname{Im} a^* d$. Since $E_0/M \simeq 10^{-4}$, one would require $\operatorname{Im} a^* d \simeq 10$ if it were to contribute an observable amount to D at the present level of experimental precision.

Our work has been motivated by the discovery of CP violation in K_L decay, which is consistent with, but by no means implies, a T-odd weak amplitude of relative size $\simeq 10^{-3}$ ("milliweak" interaction). A review of the various theoretical proposals offered to explain CP violation has been summarized by Wolfenstein.[9] A recent summary of experimental data is given by Fitch.[10]

II Experimental Method

1. Source of Polarized Neon-19

Neon 19 is produced at the LBL 88" cyclotron, transported to the experi mental apparatus, and formed into a nuclear-spin-polarized atomic beam in the $^1S_0$ atomic ground state by a method described in detail in Reference 3 (see Fig. 1). Beta decays are observed in a detector cell into which the atomic beam enters through a long narrow channel (length 7.6 cm, width 0.076 cm, height 0.95 cm). Neon-19 atoms strike the inner surfaces of the detector, fill the detector volume uniformly, and eventually decay or are pumped out of the channel into the vacuum (5×10^{-7} Torr) surrounding the cell. The sitting time in the cell is determined by the cell volume and channel conductance. It was chosen at 4 sec ($\simeq 10^{+5}$ wall collisions per atom in the

cell) to give a reasonable probability of decay within the cell without excessive loss of polarization by wall collisions, etc. The cell was designed so that observations of D could be carried out with polarization parallel or anti-parallel to the beam axis, while B observations required polarization perpendicular to the beam axis. The beam polarization as initially formed (by a "Stern-Gerlach" magnet) is transverse. This is maintained by a homogeneous magnetic field in the x direction in Fig. 1, generated by large square coils centered on the cell (not shown in Fig. 1), for B measurements. In the case of D, the polarization is rotated from transverse to longitudinal with the aid of an axial steering coil (see Fig. 1) and the magnetic field in the cell, generated by a pair of Helmholz coils 1.52 m in diameter and centered on the cell, is in the z direction and homogeneous to better than 1 part in 10^4 over the cell volume. For all measurements the sign of spin polarization can be reversed by motion of a collimating slit in the Stern-Gerlach magnet. (See Fig.2). This has negligible effect on the beam trajectory at the channel entrance, and requires no reversal of magnetic fields.

2. Detector Cell

Figures 3 and 4 show the detector cell in more detail. The hollow Aℓ frame (A in Fig. 3) on which the cell is constructed forms an octagon 2.54 cm in length with a centered 4.76 cm I.D. hole along the symmetry axis. Eight equally spaced rectangular holes are milled in the octagon as shown. On the outer octagon faces are mounted 8 Aℓ converter boxes (B) and ion dectectors (D). These assemblies face alternately in opposite directions. Lapping and silicone vacuum grease provide vacuum seals between adjoining faces. The top of each converter box, formed from a 0.005 cm Duralumin foil, provides a window through which positrons may leave the cell. Ions striking the foil stop and eject secondary electrons which are accelerated by an electrostatic field (to be described below) allowing detection of the ion. The foil is glued to the box with Shell 828 resin eposy.

The ends of the octagon are sealed by sapphire discs (E) 4.76 cm in diameter and 0.22 cm thick. Positron detectors (G) are mounted externally to the cell on a machined bracket which insures overall alignment.

The inner grid (H) is 1.90 cm long and 3.80 cm in diameter. It consists of 2 concentric cylinders of fine mesh gold-plated stainless steel screen (23.6 lines per cm, 90% transparency, manufactured by Buckbee Mears Company) mounted on the inner and outer surfaces of a metal cylinder of thickness 0.16 cm with rectangular holes. The inner grid is mounted along the bulb axis by a pin through the center of the sapphire disc and is thus electrically insulated from the rest of the cell.

The volume within the inner grid (26% of the total cell volume) is electric-field-free and is maintained at -20kV. It defines the region from which coincidence events are accepted.

The outer grid (I), formed in a similar manner from a double layer of the same stainless steel mesh, makes a slip fit in the inner hole of the Aℓ octagon. The radial distance between inner and outer grids is .4 cm. The outer grid, along with the Aℓ octagon and converter boxes, is maintained at -10keV, thus providing a 25 kV/cm potential gradient for the acceleration of F^- ions. The double-layer grid construction reduces undesirable fringing of electric fields into the interior of the inner grid and converter box. The strong E field at the surface of the inner grid might cause field emission of electrons from any microscopic metal whiskers present on the surface of the grid wires, and thus produce an undesirable background. To reduce this, both grids were gold-plated, and carefully washed in nitric acid, distilled water, and ethanol just prior to installation.

The entire detector cell unit is held by an Aℓ bracket mounted on a brass pedestal inside the 50-liter vacuum chamber, and cooled to 100° K by thermal contact with a LN_2 reservoir to reduce noise from the e^+ and ion detectors. Thermal contact to the ion detectors is maintained by the copper entrance channel and sapphire end plates (the latter being good thermal conductors but electrical insulators at LN_2 temperature).

3. Positron Detectors

Large -volume Si(Li) positron detectors are required to provide adequate solid angle and sensitive range for e^+ up to the end point energy of 2.22 MeV (range .42 cm). The dimensions of the sensitive depletion volume, 1.2 cm x 3.0 cm area by .4 cm thickness, were limited by available fabrication techniques at LBL. The detectors operate with a 400 V bias and have an energy resolution of 9 keV.

A typical coincidence e^+ energy spectrum is shown in Fig. 5. A ^{137}Cs source providing internal conversion electrons from ^{137}Ba at 625 keV and 655 keV is used for energy calibration. Discriminators are set to accept all positrons above 0.5 MeV.

4. Recoil Ion Detection

Detection of $^{19}F^-$ recoil ions requires a highly stable, efficient low noise system which, in contrast to the positron detectors, must be an integral part of the sealed cell. The ion counters, based on an earlier design[11,12] consist of a converter box with a thin secondary-emission Aℓ foil, a Si(Li) detector plus field-effect transistor pre-amplifier (FET), and a hollow glass electrical insulator separating the converter and detector boxes. The silicon detectors are 1.27 cm in diameter and 1 mm thick, and have sufficient range to stop 600-keV electrons. The sensitive depletion region is 0.96 mm thick. Cooling of the FET and detector and use of linear gates before mixing signals from all ion detectors resulted in a resolution of 4 keV. A 50Å gold layer on the detector face, chosen thin enough to allow transmission of 10 keV electrons, is maintained at a 125-V bias.

A typical coincidence event from a decay within the field-free region of the inner grid is shown in Fig. 3. The positron is detected immediately. The ion, having an average recoil energy of 100eV, drifts slowly in its original recoil direction toward the transparent surface of the inner grid, with drift times ranging from 0 to 1.4 μsec. Once the ion has passed through the inner grid it is accelerated radially toward the thin window of the converter box, which can collect ions only from the corresponding portion of the inner grid surface. After passing through the outer grid, the 10 keV ion collides at an angle of about 45° with the thin Aℓ window and ejects secondary electrons. The Si(Li) detector is sealed inside the cell and is connected with small feedthroughs to the FET in an adjoining box. With the front face of the Si(Li) detector at 125 volts and insulated from the -10keV converter box, the secondaries are accelerated and to some extent focussed toward the Si(Li) detector. An ion is thus detected as a pulse of one or more 10-keV electrons. For decays between the inner and outer grids the ions are immediately accelerated in the radial direction and detected. However these "prompt" ions are delayed less with respect to the corresponding e^+, than ions from inside the inner grid. Thus "prompt" coincidence events can be distinguished from those originating inside the inner grid.

The number spectrum of secondary electrons ejected by $^{19}F^-$ ions follows a statistical distribution with the average number emitted per stopped ion defined as the secondary emission coefficient γ; with 10 keV F^- ions on Aℓ at 45°, $\gamma \simeq 3$. For one, two, three, etc., electrons ejected, the silicon detector resolves individual lines at 10, 20, 30 keV, etc., as seen in a typical ion coincidence energy spectrum (Fig. 6). The ion discriminator was set at 15 keV to minimize the number of background events due to field emission and prompt low energy recoil ions. Thus the two-electron peak is the first one seen in Fig. 7.

III Data Collection

1. Polarization Monitoring and Singles Data.

During the "D" experiment (spin along the beam axis) continuous monitoring of ^{19}Ne polarization is achieved by using the Si(Li) ion detectors to measure the angular correlation term $A P \frac{\langle \vec{J} \rangle}{J} \cdot v$ where P is the actual polarization. A polarized ^{19}Ne atom decaying inside the cell in an appropriate region can emit a positron which passes through one of the 1-mm Si(Li) ion detectors, producing a high energy pulse. The energy lost by an e^+ of 1-2 MeV in this detector is $\simeq$ 350 keV, substantially higher than the energy from secondary electrons. With converter boxes and Si(Li) ion detectors facing alternately along the $\pm z$ axis, the difference over the sum in the high energy singles count rates, N_{Ei}, from alternate detectors, is proportional to the polarization. Specifically, the latter is given by:

$$P = [AS_A G_A \langle v \rangle]^{-1} \Delta_A \qquad (8)$$

where $A = -0.039 \pm 0.002$ is the previously measured asymmetry coefficient[3], $S_A = 0.85$ and $G_A = 0.62$ are the calculated back-scattering correction and geometry factor for this geometry respectively and $\langle v \rangle = 0.96$. Data are taken in both polarization directions ($x_c < 0$ and $x_c > 0$) and we define Δ_A by:

$$\Delta_A = \frac{1}{2} \left\{ \left(\frac{N_1 - N_2}{N_1 + N_2} \right)_{x_c>0} - \left(\frac{N_1 - N_2}{N_1 + N_2} \right)_{x_c<0} \right\} \qquad (9)$$

where $N_1(N_2)$ is the sum of the e^+ singles counts for all upstream (downstream) Si detectors for a given time. The singles data consisted of 8 channels of e^+ counts, 8 channels of ion counts and 8 channels of the 350/keV e^+ counts in the ion detectors. These data were accumulated with a 24 channel scaler system which was automatically read out into the PDP-5 computer every 15 minutes. A plot of Δ_A versus time throughout the experiment gives a measure of consistency for the polarization within the cell. (See Fig. 7).

2. Coincidence Measurements

Delayed coincidences are recorded for each position counter E and the four ion counters I oriented at ±90° and ±135° with respect to E. (See Fig. 8 and Table 1a, 1b.) For example, in the "D" experiment the ^{19}Ne nuclear spin is oriented along the ±z directions. Thus for a given spin direction a finite D would lead to different coincidence counting rates for E_1, I_4, and E_1, I_6. In Table 1a, (E_1, I_4) is called the first "regular" pair (135°) and (E_1,I_6) is its corresponding "image" for the D experiment. Similarly (E_1, I_3) is the ninth "regular" pair (90°) and(E_1,I_7) is its corresponding "image" pair. In the "B" experiment the ^{19}Ne spin is oriented along the x-axis and a different combination of "regular" and "image" pairs is required (see Table 1b).

Together with each coincidence event, the following information is recorded: the label identifying the coincidence pair, the time delay t between positron and ion, and their respective energies E_e and E_I. (See Fig. 9).

Coincidence rates together with the uncorrelated positron and ion singles rates, are accumulated for 15-min intervals in each of the nuclear polarization states (collimator positions $x_c>0$ and $x_c<0$). A three minute measurement of the background, made by moving the collimator far to one side and thus blocking the Ne^{19} beam, completes each measurement sequence.

Coincidences are accepted with ion delay times between 0 μsec and 4 μsec, as taken on a 5 μs scale of a time-to-amplitude converter (TAC) with ion signals delayed by 1 μsec to shift the zero. Three types of coincidence events are distinguished: prompts, trues, and accidentals. (See Fig. 10.) As previously noted, prompts result from decays between the 10 kV and 20 kV grids. No correlation between e^+ and ion directions is possible, and these events (sharply peaked between 1.0 and 1.5 μs) provide no useful D or B information. True coincidence events result from decays inside the inner (20 kv) grid.

Here, correlation information is preserved and delay times in the acceptable range are from 1.6 to 2.6 μs, depending on the drift path. Prompts and trues can be distinguished, since their overlap in time is small. Accidental coincidences are uniformly distributed in time, and their contribution can be measured by holding the coincidence gate open for times before and after the time interval when trues are expected (0-1 μs, 3-5 μs).

Typical coincidence counting rates per 135° pair were .7 counts/sec and .2 counts/sec for trues and accidentals, respectively. Typical singles rates per counter were $N_{e^+} = 130$ counts/sec, and $N_I = 2000$ counts/sec, corresponding to a disintegration rate of about 10^4/sec in the cell.

IV Data Analysis and Results

1. D Experiment

We consider the positron-ion coincidence pairs ℓ as given in Table 1a for D. Let the measured coincidence counts corrected for background for the regular and image pairs be y_ℓ and y'_ℓ, respectively. We form the quantities

$$\Delta_D^{135} = \frac{1}{16} \sum_{\ell=1}^{8} \left\{ \left(\frac{y_\ell - y'_\ell}{y_\ell + y'_\ell} \right)_{x_c>0} - \left(\frac{y_\ell - y'_\ell}{y_\ell + y'_\ell} \right)_{x_c<0} \right\} \tag{10}$$

and

$$\Delta_D^{90} = \frac{1}{16} \sum_{\ell=9}^{16} \left\{ \left(\frac{y_\ell - y'_\ell}{y_\ell + y'_\ell} \right)_{x_c>0} - \left(\frac{y_\ell - y'_\ell}{y_\ell + y'_\ell} \right)_{x_c<0} \right\} \tag{11}$$

by combining the coincidence observations into experimental asymmetries Δ in this manner, we introduce a high degree of symmetry into the analysis which eliminates the possibility of systematic errors due to unequal counter efficiencies or possible slight spin misalignment (false B effect).[1,3]

We then compute D from the formula

$$D = \frac{1}{2} \frac{1}{PS} \left[\frac{1}{G_D^{90}} \Delta_D^{90} + \frac{1}{G_D^{135}} \Delta_D^{135} \right] \tag{12}$$

where P is the polarization, S is a backscattering correction, and the G's are geometry factors for the 90° and 135° coincidence pairs. These geometry factors account for the finite spatial volume of the detectors, the finite decay volume, and the momentum distribution of the decay products. A Monte Carlo calculation yields $G_D^{90} = 0.67 \pm 0.03$ and $G_D^{135} = 0.42 \pm 0.02$ for the inner grid used on 5 cyclotron runs, while $G_D^{90} = 0.77 \pm 0.04$ and G_D^{135} 0.56 ± 0.03 for an inner grid of smaller diameter used on one cyclotron run.

Total running time for the D measurement was 125 hours, during which 4×10^6 D events were collected in ~215 separate polarization cycles. For all of the final D data $P = 0.75 \pm 0.05$ from A measurements quoted earlier, and $S = 0.80 \pm 0.14$ as determined from B measurements (see below). The final D data was separated into 3 e^+-energy intervals: δE_1 = 0.5 to 1.0 MeV, δE_2 = 1.0 to 1.5 MeV, δE_3 = 1.5 to 2.21 MeV. Here 0.5 MeV and 2.21 Mev are the threshold and endpoint energies respectively. We find:

$$D(\delta E_1) = -0.009 \pm 0.006$$
$$D(\delta E_2) = +0.008 \pm 0.005$$
$$D(\delta E_3) = +0.010 \pm 0.011$$

No energy-dependent trend or significant difference exists between these values of D. (See Fig. 11 which also shows the predicted energy dependence of D for an assumed value of the induced tensor term d). Either by combining these values of D or by taking the weighted averages of D's as computed from Δ_D^{90} and Δ_D^{135} for all energies between threshold and endpoint, we obtain

$$D = 0.001 \pm 0.003 \qquad (13)$$

The quoted uncertainty in D is purely statistical.

2. B Experiment

Referring to Table 1b, let the observed counts for the n'th regular and image pairs be ξ_n and ξ_n' respectively. We define:

$$\Delta_B(1,2) = \frac{1}{4} \sum_{n=1}^{2} \left\{ \left(\frac{\xi_n - \xi_n'}{\xi_n + \xi_n'} \right)_{x_c>0} - \left(\frac{\xi_n - \xi_n'}{\xi_n + \xi_n'} \right)_{x_c<0} \right\} \qquad (14)$$

with similar expressions for $\Delta_B(3,4)$, $\Delta_B(5,6)$ and $\Delta_B(7,8)$. Since in the B experiment, the ^{19}Ne spin lies along the x-axis, the D correlation averages to zero and the coincidence rate ξ for a given pair depends on B, but also for n = 3, 4, 7, 8 it depends on A. The magnitude of A is known from previous experiments; thus B can be determined from the expressions:

$$135^\circ \text{ pairs} \begin{cases} BG_B^1 = \frac{1}{PS}\,\Delta_B(1,2) & (15) \\ (BG_B^2 + AG_{BA}^1) = \frac{1}{PS}\,\Delta_B(3,4) & (16) \end{cases}$$

$$90^\circ \text{ pairs} \begin{cases} BG_B^3 = \frac{1}{PS}\,\Delta_B(5,6) & (17) \\ (BG_B^4 + AG_{BA}^2) = \frac{1}{PS}\,\Delta_B(7,8) & (18) \end{cases}$$

Actually, since B was already known from previous work, the B measurement serves only as a check on the design and operation of the dete tor-cell system. A high degree of accuracy is unnecessary, and only $\Delta_B(1,2)$ was actually determined by measurements accumulated over a total of $\sim$10 hours. The value of Δ_B obtained for all positron energies between 0.5 and 2.21 MeV and delay times between 1.6 μs and 2.6 μs is

$$\Delta_B = -0.258 \pm 0.015 \qquad (19)$$

Using P= 0.75 ± 0.05, S = 0.85 ± 0.1 and G_B^1 = 0.48 ± 0.03 we obtain:

$$B = -0.85 \pm 0.17 \qquad (20)$$

in agreement with our previous value[3]

$$B = -0.90 \pm 0.13 \qquad (21)$$

measured by the decay-in-flight method.

The uncertainties are attributable to uncertainties in P, G, and particularly to S, rather than to statistics. Note that from eq. (4) and $|\rho| = 1.60$ with $\phi \approx 180°$, $^{B}_{theo} = -.998$.

Alternatively, one may use our present B result as a measure of e^+ (and F^-) backscattering in the extremely complex cell geometry. For this purpose we write:

$$S = S_e S_I = \frac{(\Delta_B)}{G_B P\ |B|} \tag{22}$$

where $|B| = 0.90 \pm 0.13$. The quantities S_e and S_I are scattering correction factors for positions and ions respectively. The latter quantity is difficult to predict but is determined together with S_e by measuring Δ_B. Inserting $P = 0.75$, $G_B = 0.48$, we find

$$S = 0.80 \pm 0.14$$

which we assume is valid for the backscattering correction in the D experiment also.

V. Conclusions

From equations (5), and (13), with $|\rho(^{19}Ne)| = 1.60$, we obtain for the phase angle between axial vector and vector amplitudes in ^{19}Ne decay:

$$\phi_{A,V} = 180.1 \pm 0.3° \tag{23}$$

This represents a factor of five improvement over our previous result. The quoted error is purely statistical.

Unfortunately the present result is inadequate in precision to test the hypothesis that there exists a T-odd amplitude of relative size 10^{-3} in the weak interaction. To make this test it would be necessary to improve our precision by an order of magnitude, and although we regard this as desirable, it would be totally impractical without major improvements in the present experimental apparatus. Mere increase in the total disintegration rate in the detector cell would not lead to a significant improvement because of rapid increase in the ratio of accidental-to-true coincidences

However a large increase in the size of the e^+ detectors and a consequent improvement in effective solid angle together with a more efficient data-handling-system could possibly lead to a 10-fold reduction in the uncertainty in D.

Acknowledgements

We are very grateful to M. Simmons for his valuable assistance with many aspects of this experiment. We also wish to thank H. Shugart, M. Prior, B. Harvey, F. Goulding, D. Landis and D. Lundgren for very useful advice and assistance.

References

1. See also D. C. Girvin, Thesis, University of California , 1972 (LBL report #731, unpublished)
2. F. P. Calaprice, E. D. Commins, H. M. Gibbs, G. L. Wick, and D. A. Dobson, Phys. Rev. Letters 18, 918, (1967).
3. F. P. Calaprice, E. D. Commins, H. M. Gibbs, G. L. Wick, and D. A. Dobson, Phys. Rev. 184, 117 (1969)
4. B. J. Erozolimski et.al., Sov. J. Nucl. Phys. 11, 583 (1970)
5. J. D. Jackson, S. B. Treiman and H. W. Wyld, Jr. Phys. Rev. 106, 517, (1957)
6. B. R. Holstein, Phys. Rev. C 5, 1529 (1972)
7. E. D. Commins, Weak Interactions, p.96, McGraw Hill, New York (1973)
8. C. W. Kim and H. Primakoff, Phys. Rev. 180, 1502 (1969), also L. Ma iani, Phys. Letters 26B, 538 (1968) and N. Cabibbo, Phys. Letters 12, 137 (1964)
9. L. Wolfenstein, in Theory and Phenomenology of Particle Physics, P.218, ed. A. Zichichi, Academic Press, New York and London (1969)
10. V. Fitch, Princeton University Internal Report PURC-4159-53 (1972)
11. H. M. Gibbs and E. D. Commins, Rev. Sci. Instr. 37, 1385, (1966)
12. F. Calaprice and P. Goldsmith, to be published.

Table 1 Positron-Ion Coincidence Pairs

a) Regular and image coincidence pairs for "D" experiment.

	Pair Index ℓ	Regular Pair	Image Pair	Geometry Factor
		Counters e^+ F^-	Counters e^+ F^-	
135° pairs	1	1:4	1:6	G_D^{135} =
	2	5:8	5:2	
	3	7:2	7:4	0.42 ± 0.03
	4	3:6	3:8	
	5	2:5	8:5	
	6	6:1	4:1	
	7	8:3	6:3	
	8	4:7	2:7	
90° pairs	9	1:3	1:7	G_D^{90} =
	10	5:7	5:3	
	11	3:5	3:1	0.67 ± 0.03
	12	7:1	7:5	
	13	8:2	2:8	
	14	4:6	6:4	
	15	2:4	4:2	
	16	6:8	8:6	

Table 1 (Continued)

b) Regular and image coincidence pairs for "B" experiment.

	Pair Index n	Regular Pair	Image Pair	Geometry Factor
		Counters e^+ F^-	Counters e^+ F^-	
135° pairs	1	1:4	1:6	G_B^1 =
	2	5:2	5:8	0.48 ± 0.03
	3	4:1	6:1	
	4	2:5	8:5	
90° pairs	5	1:3	1:7	G_B^3 =
	6	5:3	5:7	0.77 ± 0.04
	7	3:1	7:1	
	8	3:5	7:5	

Figure 1. Schematic diagram of apparatus (not to scale). ^{19}Ne is produced by reaction $^{19}F(p,n)^{19}Ne$ with 15 MeV protons from LBL 88" cyclotron in target containing SF_6 gas at ~1.5 atm pressure. SF_6 is continuously circulated through target and carries ^{19}Ne to an LN_2 trap where SF_6 is removed. Target and experimental areas are separated by massive concrete shielding. ^{19}Ne continues from trap to atomic beam source at 30°K. Beam is formed by effusion from slit S_1 and collimated by slit S_3, the position of which determines m_I: dark (light) arrows represent orientation of ^{19}Ne nuclear moment (antiparallel to spin) as atoms pass through S_3 for $\chi_c > 0$ (< 0). Moments follow adiabatically the changing orientation of magnetic fields. In "D" experiment spins are rotated from transverse to longitudinal orientation with axial coil. In "B" experiment spins remain transverse. Beam deflections are grossly exaggerated for clarity. Actual collimator deflection on either side of center line is .076 cm, while beam length is about 1.5 m.

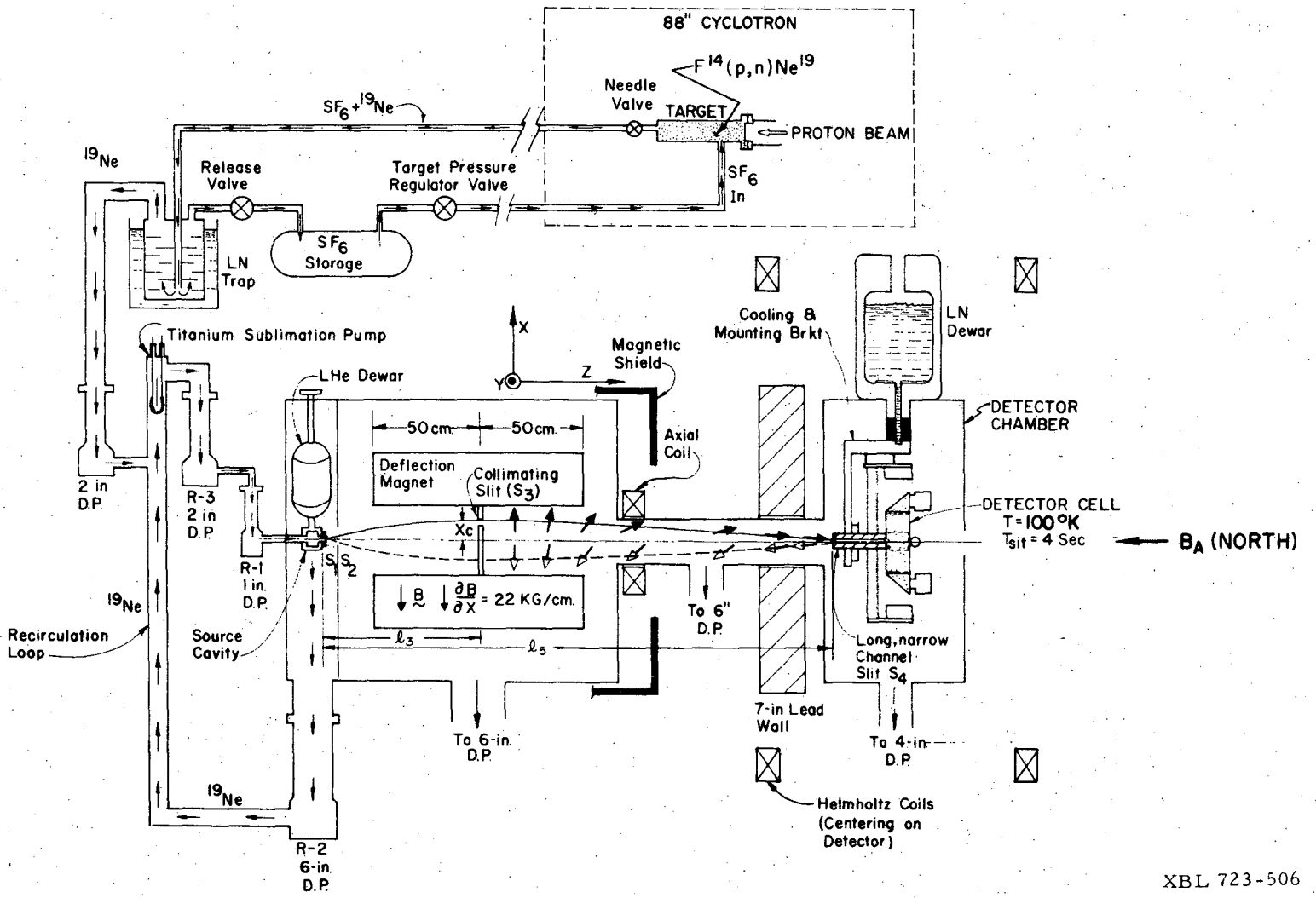

XBL 723-506

Fig. 1

Figure 2 caption. Beam intensity and polarization at entrance to detector cell. The solid curves are calculated using $\mu(^{19}Ne) = -1.88\mu_N$, a source temperature of 30°K, and a deflection magnetic field gradient of 22 kG/cm. Experimental points are shown as triangles and squares. x_c is the distance from the magnet center line to the center of the collimating slit, which is .076 cm wide. For $x_c > 0.076$ cm the polarization of the beam is 100%. Arrows indicate locations of the collimator slit center line used to select opposite spin states in actual experiment.

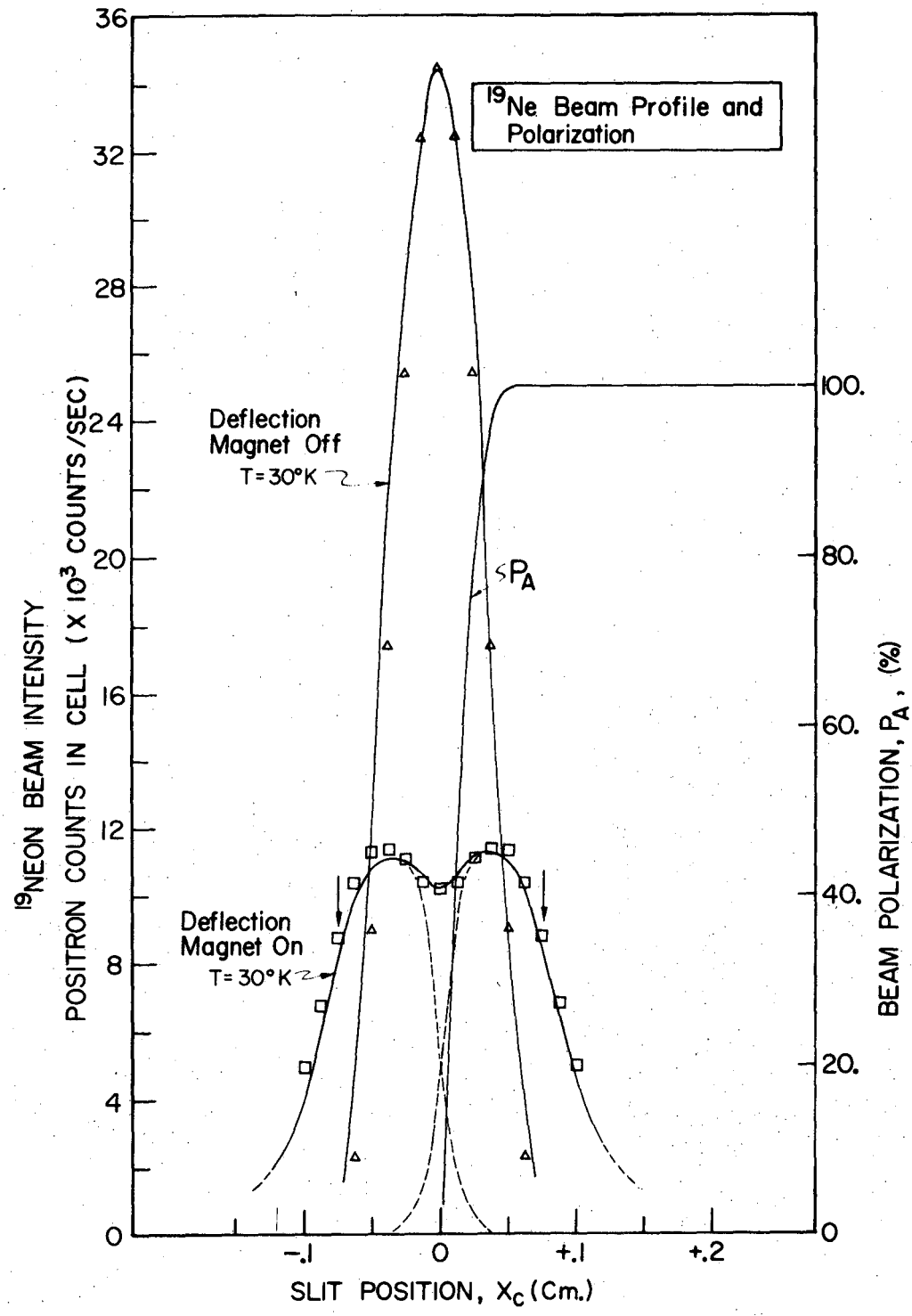
^{19}Ne Beam Profile and Polarization
Deflection Magnet Off
T=30°K
Deflection Magnet On
T=30°K
P_A
^{19}NEON BEAM INTENSITY
POSITRON COUNTS IN CELL (X 10^3 COUNTS/SEC)
BEAM POLARIZATION, P_A, (%)
SLIT POSITION, X_c (Cm.)
36
32
28
24
20
16
12
8
4
0
100.
80.
60.
40.
20.
0
-.1
0
+.1
+.2
XBL 723-574

Fig. 2

Figure 3. Side and end view of octagonal cell detector assembly. Converter boxes are shown in end view as rectangles mounted on octagon, with openings to Si detectors alternately facing along ±z axis. Inner and outer grids are shown as double dashed lines.

Detector functions in D experiment as follows. After entering cell through long narrow copper channel, ^{19}Ne atoms (shown as dots) are uniformly distributed throughout cell volume. Particle trajectories from a typical decay within inner grid are shown in both views. Positron passes through foil, while ion drifts radially toward edge of inner grid. Radial acceleration of ion is followed by secondary electron (e^-) production upon ion impact with foil. The nuclear spin of ^{19}Ne, denoted as P, is maintained by a magnetic field $\underset{\sim}{B}_A = \pm \hat{\underset{\sim}{z}}|B_A|$. Positrons originating from decays within converter boxes and passing through the Si (secondary-electron) detectors provide a 350-keV signal. Such a decay is shown at top left. Measurement of these 350-keV singles counts provides continuous monitoring of polarization.

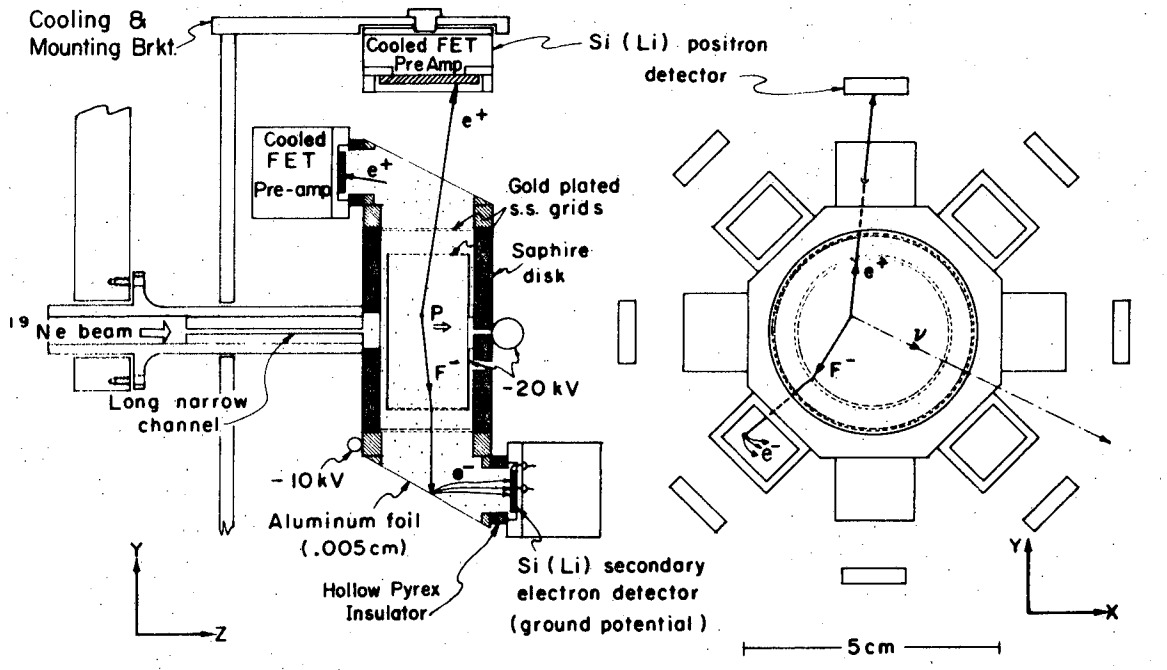
Cooling &
Mounting Brkt.
Cooled FET
PreAmp
Si (Li) positron
detector
e+
Cooled
FET
Pre-amp
e+
Gold plated
s.s. grids
Saphire
disk
19Ne beam
P
F-
-20 kV
Long narrow
channel
-10 kV
e-
Aluminum foil
(.005 cm)
Hollow Pyrex
Insulator
Si (Li) secondary
electron detector
(ground potential)
Y
Z
e+
ν
F-
e-
Y
X
5 cm
XBL707-3359A

Fig. 3

Figure 4. Exploded view of cell detector assembly. Sapphire discs are held onto octagon by small brass spring clips. Other items are secured with screws. All joining surfaces are lapped to flatness. Dow Corning silicon-based vacuum grease is used to ensure a vacuum seal of all joints. A copper lip, threaded into the end of the copper beam entrance channel, secures sapphire disc. The only opening in the bulb is the 0.07x0.95-cm entrance slit. When all joints are properly sealed the sitting time of the ^{19}Ne in the bulb is 4 sec.

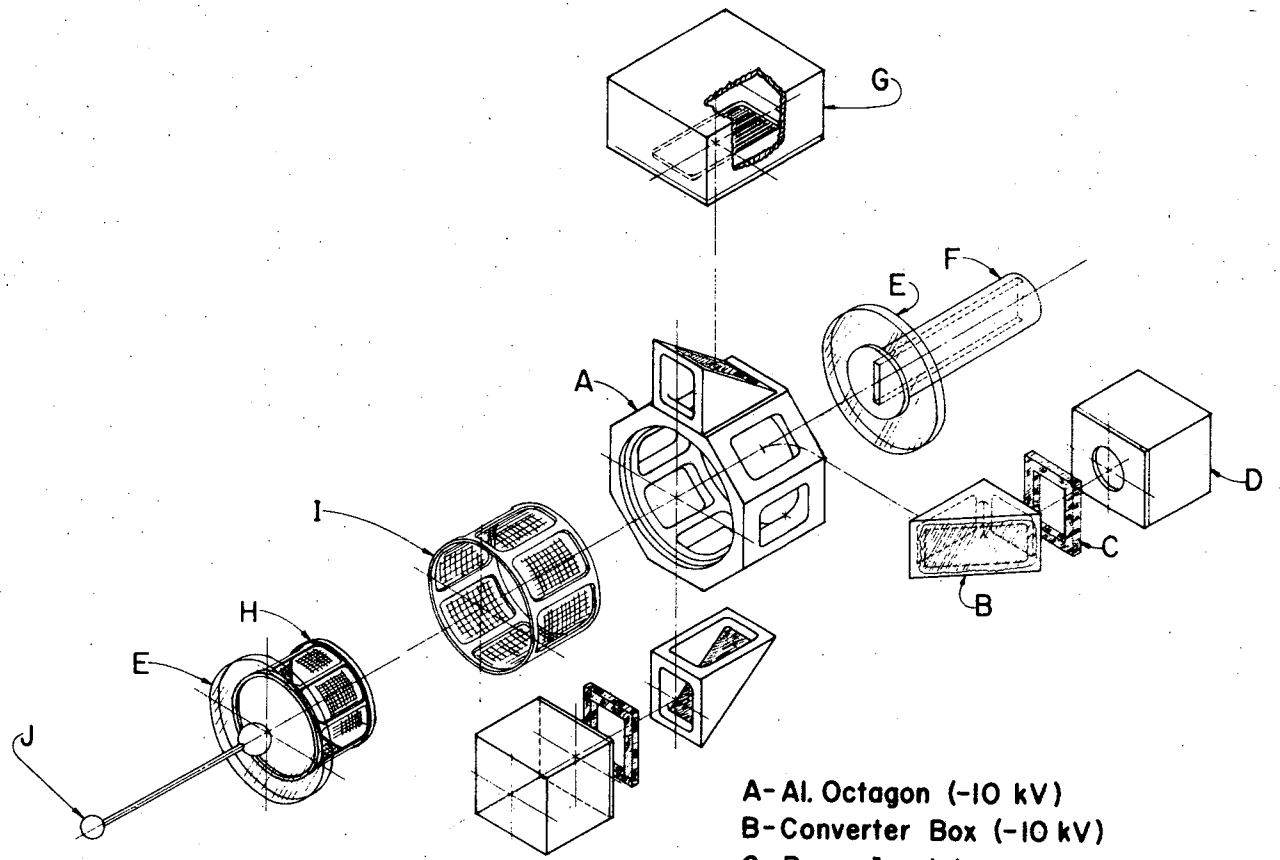

A-Al. Octagon (-10 kV)
B-Converter Box (-10 kV)
C-Pyrex Insulator
D-Ion Detector & FET Box (Ground Potential)
E-Sapphire Discs
F-Beam Entrance Channel (Ground Potential)
G-Positron Detector & FET Box (Ground Potential)
H-Double Layer Inner Grid (-20 kV)
I-Double Layer Outer Grid (-10 kV)
J-20kV High Voltage Connector

XBL 723-505

Fig. 4

Figure 5. Observed positron energy spectrum for e^+ in coincidence with $^{19}F^-$. Peak at 340 keV is due to electrons in detector which have suffered a single Compton-scattering with incoming annihilation photons, (.511 Mev). The dashed vertical line corresponds to the discriminator setting.

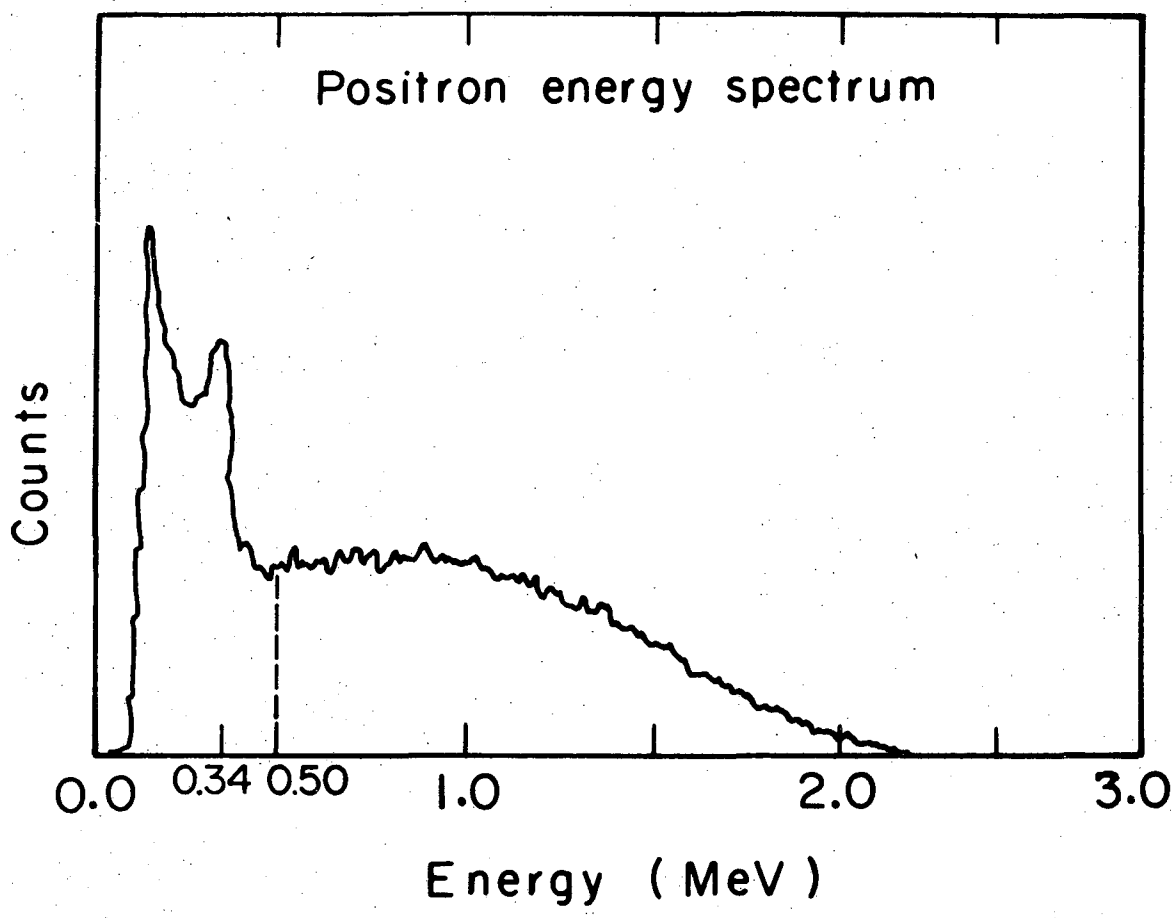

XBL 707-3357A

Fig. 5

Figure 6. Secondary electron spectrum generated by collision of $^{19}F^-$ ions with detector foil, in $e^+ - F^-$ coincidence events. For B and D data, ion energy discriminator was set at 15 keV to eliminate large number of single secondary electrons produced by prompt recoil ions.

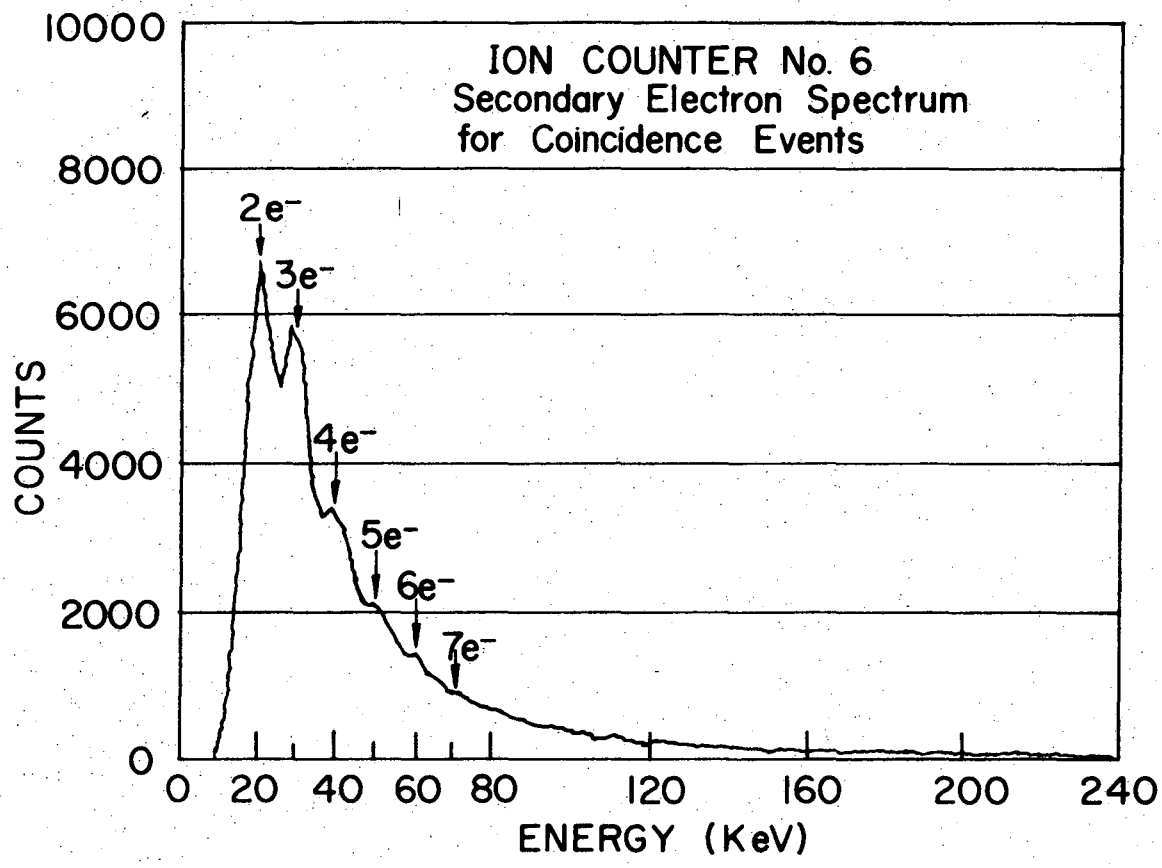

XBL 723-513

Fig. 6

Figure 7. Absolute value of polarization asymmetry ΔA, plotted versus timer run. ΔA values for cyclotron run no. 0 were lower than in other runs because of poor uniformity and low magnitude of alignment field B_A. These conditions were improved for subsequent runs, and run no. 0 data was not used for determining B and D. D data was not used for any timer run whose values of $|\Delta A|$ deviated by more than 2σ from the experimental average of $(1.52 \pm 0.01) \times 10^{-2}$.

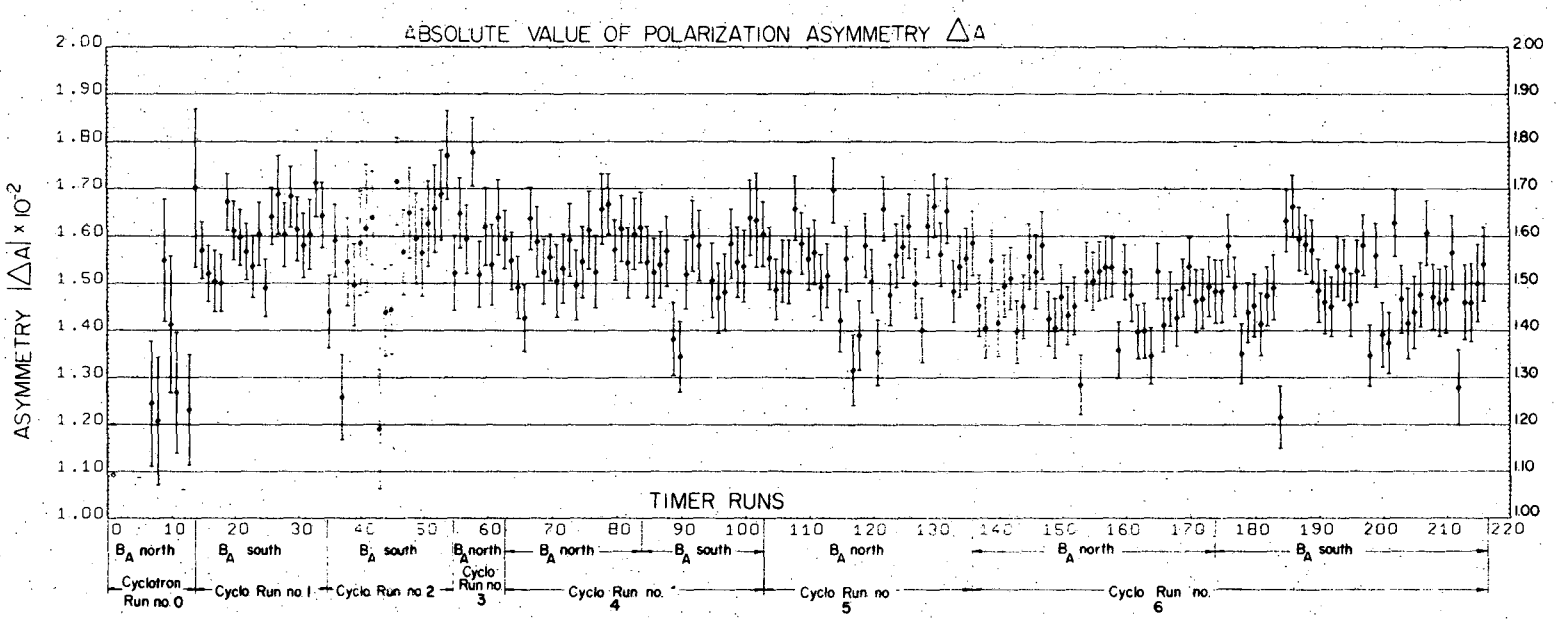
ABSOLUTE VALUE OF POLARIZATION ASYMMETRY △A
ASYMMETRY |△A| x 10⁻²
2.00
1.90
1.80
1.70
1.60
1.50
1.40
1.30
1.20
1.10
1.00
TIMER RUNS
0 10 20 30 40 50 60 70 80 90 100 110 120 130 140 150 160 170 180 190 200 210 220
B_A north
B_A south
B_A north
Cyclotron Run no 0
Cyclo Run no 1
Cyclo Run no 2
Cyclo Run no 3
Cyclo Run no. 4
Cyclo Run no 5
Cyclo Run no. 6
XBL 723-508

Fig. 7

Figure 8. Schematic view of detector octagonal counter geometry. Positron and ion counter designations E_i and I_j provide a key to counter pair numbering in Table 1.

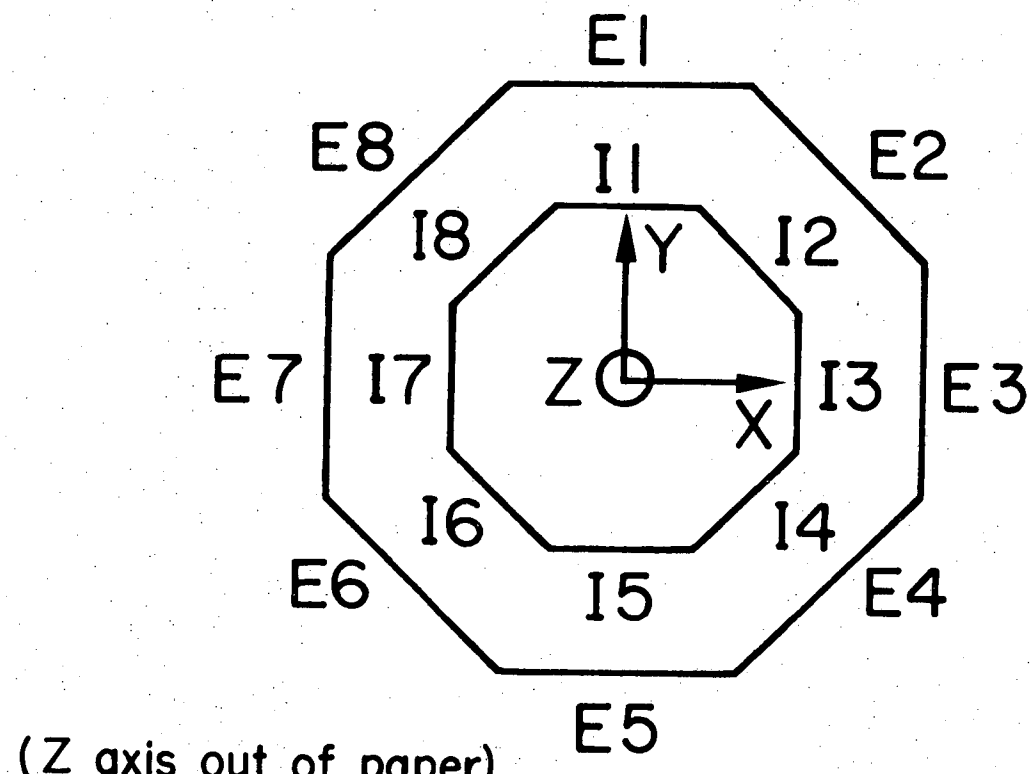

XBL 723-573

Fig. 8

Figure 9. Schematic diagram of electronics and data transfer system. For each e^+ above 0.5 MeV threshold in E_i, fast logic pulse registers singles count, sets identification (ID) register labeling count as coming from E_i, gates off acceptance of all additional e^+ coincidence starts, and starts time-to-amplitude converter (TAC) for determination of time delay for possible coincidence. Signal level (energy E_e) from positron preamp is routed to and held in multiplexer until ion completes coincidence. If no coincidence occurs within 5 μs, multiplexer and ID register are cleared and e^+ gate opens.

Ion pulse I_j causes fast and slow linear amplifier output. Above ion threshold (2 secondary electrons = 20 keV) fast output registers ion singles count, sets j'^{th} ion ID register, gates off acceptance of all additional ion coincidence stops, and stops TAC, thus registering coincidence. Fast ion pulse also gates slow ion signal (energy E_I) from linear amp into multiplexer. For coincidence, TAC provides multiplexer with time delay Δt. On-line computer analysis of incoming coincidence data is major source of deadtime in system. Dead-time approached 50% at highest counting rates.

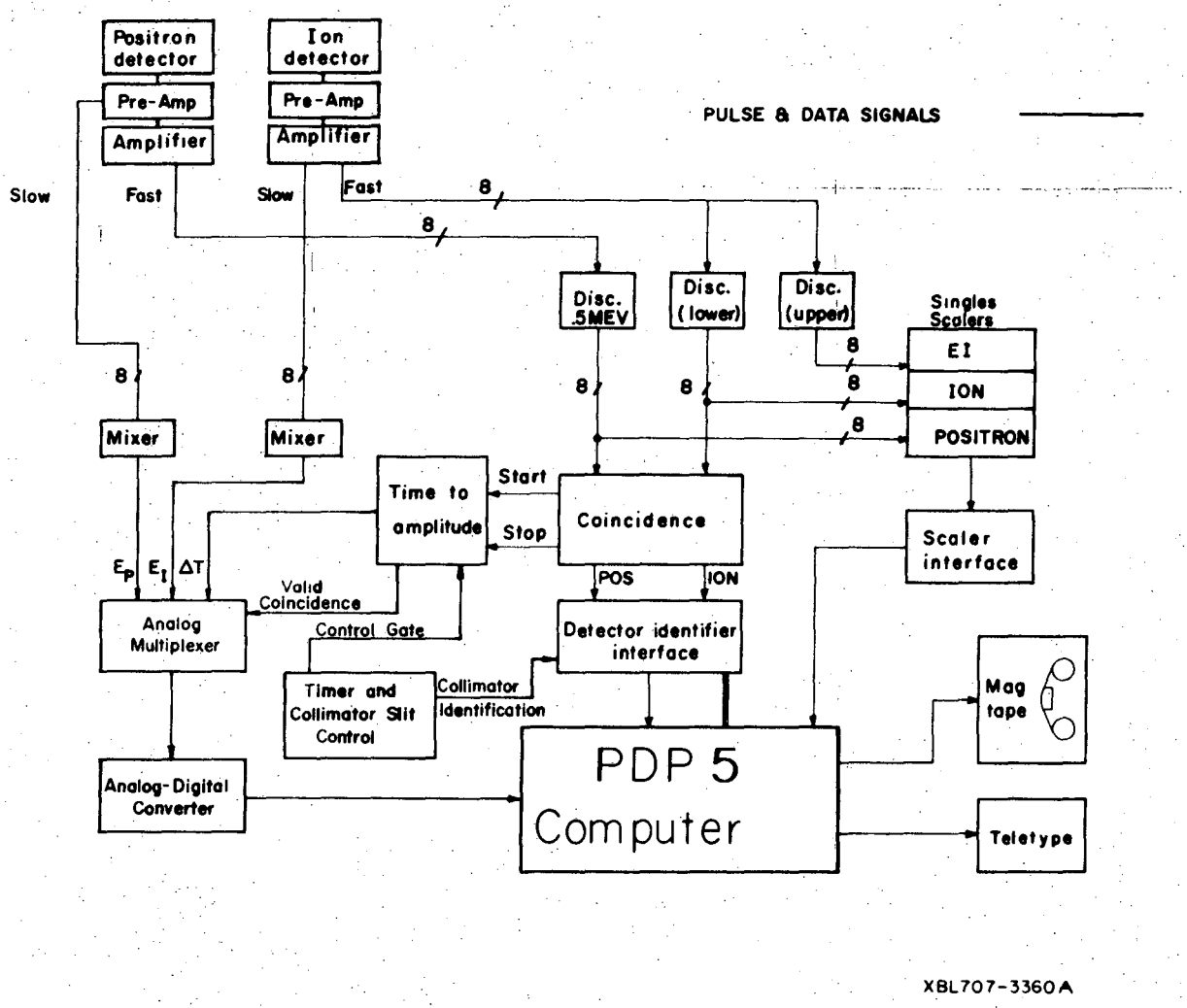
Positron detector
Ion detector
Pre-Amp
Pre-Amp
Amplifier
Amplifier
PULSE & DATA SIGNALS
Slow
Fast
Slow
Fast
8
8
Disc. .5MEV
Disc. (lower)
Disc. (upper)
Singles Scalers
EI
ION
POSITRON
Mixer
Mixer
Time to amplitude
Start
Stop
Coincidence
Scaler interface
E_P E_I ΔT
Valid Coincidence
POS
ION
Analog Multiplexer
Control Gate
Detector identifier interface
Timer and Collimator Slit Control
Collimator Identification
Mag tape
PDP 5 Computer
Analog-Digital Converter
Teletype
XBL707-3360A

Fig. 9

Figure 10. Time distribution of coincidence events for typical 135° pair, with large inner grid, used for most of D data. Prompt events are caused by ions originating between inner and outer grids; these are useless for measuring D or B. Prompt and true events overlap in region between 1.2 and 1.5 μsec. Only true events in region between 1.6 and 2.6 μs were accepted for analysis. Similar time distributions were observed for the small inner grid, and for 90° e^+ - F^- counter pairs.

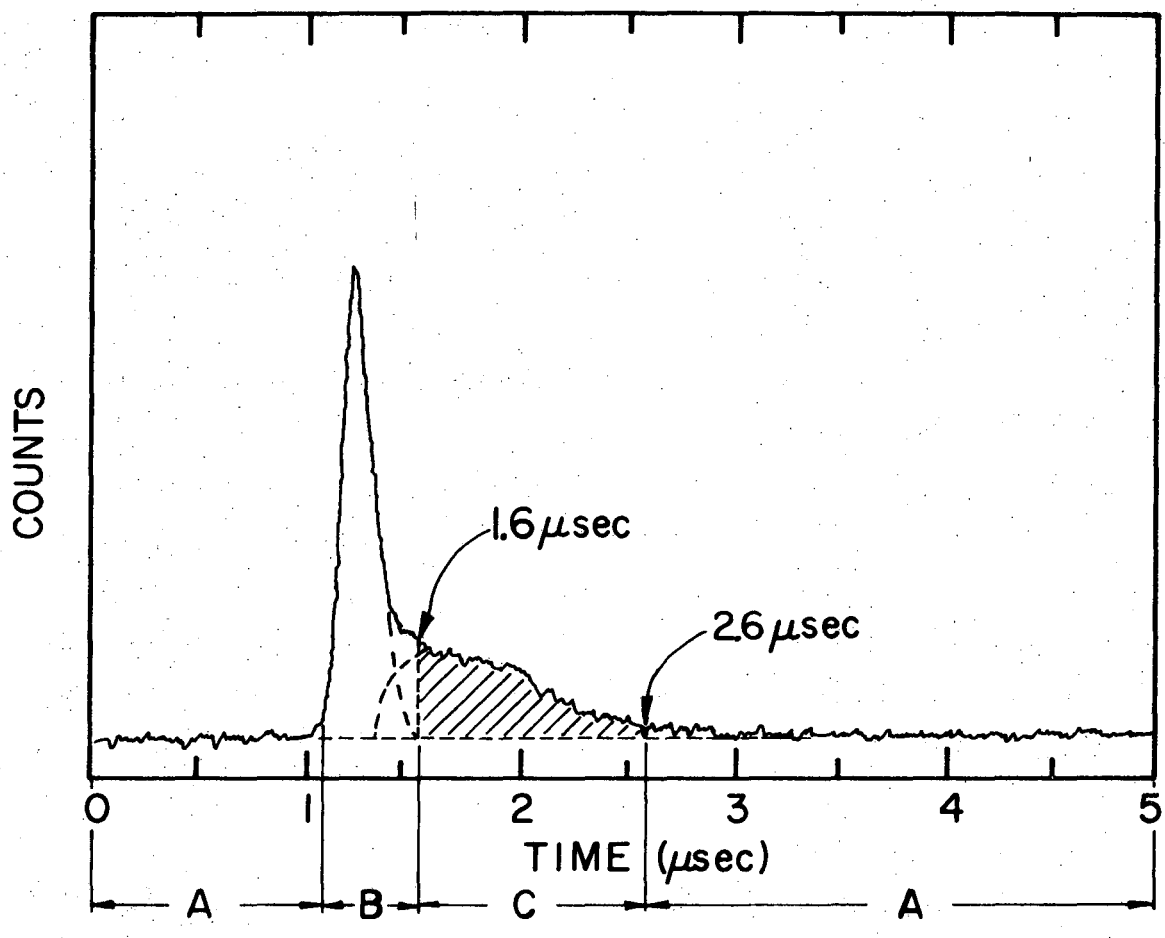
COUNTS
1.6 μsec
2.6 μsec
0
1
2
3
4
5
TIME (μsec)
A
B
C
A
A - Accidental Background
B - Prompt+Background
C - True+Background
XBL 723-512

Fig. 10

Figure 11. Theoretical D is plotted vs. electron kinetic energy T in units of maximum kinetic energy T_o = 2.21 MeV (dashed line) assuming Im a_d^* = 10, Im a_c^* = 0, and the CVC hypothesis. The points with vertical error bars correspond to measurements of D for the energy intervals δE_1, δE_2, δE_3 as defined in text.

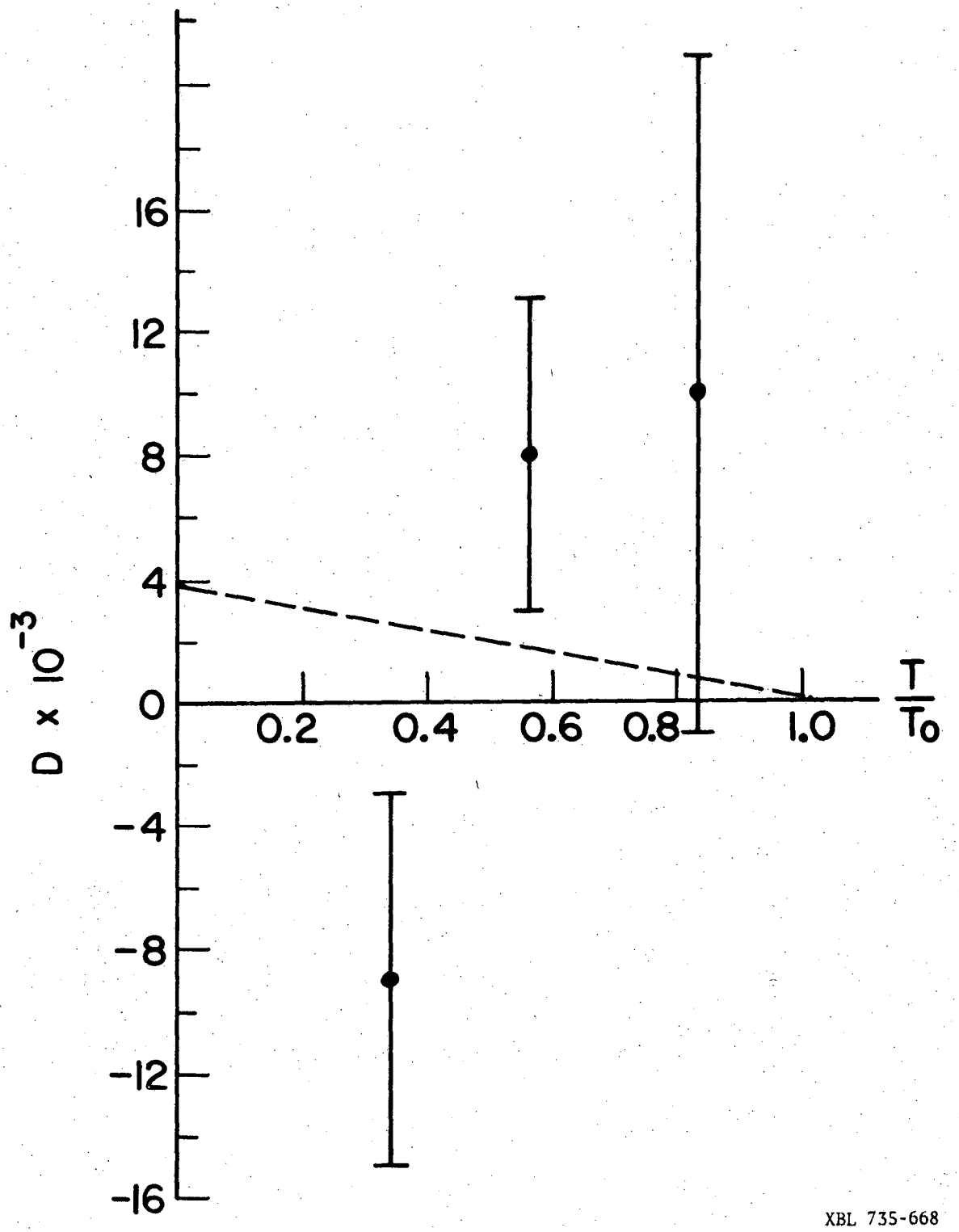

Fig. 11

TECHNICAL INFORMATION DIVISION
LAWRENCE BERKELEY LABORATORY
UNIVERSITY OF CALIFORNIA
BERKELEY, CALIFORNIA 94720